Electronic excitations and structure of Li_2IrO_3 thin films grown on ZrO_2:Y (001) substrates

Marcus Jenderka, Rüdiger Schmidt-Grund, Marius Grundmann, and Michael Lorenz

Citation: Journal of Applied Physics **117**, 025304 (2015); doi: 10.1063/1.4905790
View online: https://doi.org/10.1063/1.4905790
View Table of Contents: http://aip.scitation.org/toc/jap/117/2
Published by the American Institute of Physics

JOURNAL OF APPLIED PHYSICS **117**, 025304 (2015)

Electronic excitations and structure of Li_2IrO_3 thin films grown on ZrO_2:Y (001) substrates

Marcus Jenderka,[a] Rüdiger Schmidt-Grund, Marius Grundmann, and Michael Lorenz
Institut für Experimentelle Physik II, Universität Leipzig Linnéstraße 5, D-04103 Leipzig, Germany

(Received 10 September 2014; accepted 30 December 2014; published online 12 January 2015)

Thin films are a prerequisite for application of the emergent exotic ground states in iridates that result from the interplay of strong spin-orbit coupling and electronic correlations. We report on pulsed laser deposition of Li_2IrO_3 films on ZrO_2:Y (001) single crystalline substrates. X-ray diffraction confirms preferential (001) and (10-1) out-of-plane crystalline orientations with well defined in-plane orientation. Resistivity between 35 and 300 K is dominated by a three-dimensional variable range hopping mechanism. The dielectric function is determined by means of spectroscopic ellipsometry and, complemented by Fourier transform infrared transmission spectroscopy, reveals a small optical gap of ≈300 meV, a splitting of the $5d$-t_{2g} manifold, and several in-gap excitations attributed to phonons and possibly magnons. © *2015 AIP Publishing LLC*.
[http://dx.doi.org/10.1063/1.4905790]

I. INTRODUCTION

The layered perovskite oxides A_2IrO_3 (A = Na, Li) have in recent years been studied in terms of a physical realization of the Kitaev and Heisenberg-Kitaev model and its extensions, harboring spin liquid, and topologically ordered phases.[1–6] They have also drawn interest as possible topological insulators.[7–10] Ultimately, the physical realization of such states of matter is desired with respect to quantum computation proposals.[11–13] Subsequently, experiments showed that both materials order magnetically at ≈15 K: Na_2IrO_3 is deep within an antiferromagnetically zig-zag ordered phase,[14–17] whereas Li_2IrO_3 shows incommensurate spiral order but is placed close to the desired spin liquid phase.[5,6,18] There is yet no direct experimental evidence of a topological insulator phase in either of the two materials.

Some of us have previously reported on the first successful growth of heteroepitaxial Na_2IrO_3 thin films, where we observed three-dimensional variable range hopping (VRH) conductivity and the weak antilocalization effect in magnetoresistance.[19] To date, available single crystals are of very small size, such that experimental data on Li_2IrO_3 is often restricted to powder-averaged data.[5,18,20,21] Certain types of experiments, such as terahertz pump-probe spectroscopy or neutron diffraction, benefit from large-area single-crystalline thin film samples. Neutron diffraction experiments, for instance, are challenging because of a high absorption cross-section of iridium and the small crystal sizes. Thin films, however, alleviate these problems by distributing the volume over a large area. If its growth was feasible, thin films would, in general, also allow for the study of strain-induced effects. In fact, both a strain-induced spin liquid and topological insulator phase are proposed to exist.[4,5,9,10] Hence, thin films of this class of material lay a foundation for future experiments including, e.g., studies on the $(Na_{1-x}Li_x)_2IrO_3$ compounds, which are not available in single crystalline form so far.

Like its sister compound Na_2IrO_3, Li_2IrO_3 is an antiferromagnetic insulator with Neél temperature $T_N \approx 15$ K below which it orders in an incommensurate spiral fashion.[5,6,18] X-ray powder diffraction measurements suggest a monoclinic C2/c unit cell.[5,18] Temperature dependent resistivity shows insulating behavior between 100 and 300 K.[5] A delicate interplay between trigonal distortions of the IrO_6 octaeder and spin-orbit coupling causes the spin-orbit assisted Mott insulating state. Until recently, the magnitude of the trigonal distortions was unclear. Consequently, the adequate description of the underlying electronic structure was under debate.[22–24] However, recent resonant inelastic x-ray scattering (RIXS) experiments[21] validate the applicability of the so-called j_{eff} physics in Li_2IrO_3, which in the past was applied to Sr_2IrO_4 and related materials:[25–28] The cubic crystal field caused by the edge-sharing IrO_6 octaeder splits the Ir $5d$ orbitals into a e_g doublet and a t_{2g} triplet. The splitting between e_g and t_{2g} is about 3 eV.[29] Structural distortions of the monoclinic unit cell and the oxygen tetraeder, respectively, create a trigonal crystal field. If this field is sufficiently small compared to spin-orbit coupling, the t_{2g} triplet further splits into a fourfold degenerate $j_{eff} = 3/2$ and a twofold degenerate $j_{eff} = 1/2$ band.

In this paper, we report on the pulsed laser-deposition (PLD) of Li_2IrO_3 thin films and the study of their structure. Temperature-dependent resistivity is measured between 300 and 25 K. Employing spectroscopic ellipsometry, we determine the dielectric function (DF) in order to study and interpret low energy electronic excitations on the basis of j_{eff} physics. These results are complemented with optical transmission data measured with a Fourier transform infrared spectrometer (FTIR).

II. EXPERIMENTAL DETAILS

Li_2IrO_3 thin films were grown by PLD on 10×10 mm^2 ZrO_2:Y (001) single crystals (YSZ). PLD was done with a

[a]Author to whom correspondence should be addressed. Electronic mail: marcus.jenderka@physik.uni-leipzig.de.

248 nm KrF excimer laser at a laser fluence of 2 J cm^{-2}. The phase-pure polycrystalline target was prepared by a solid state synthesis of Li_2CO_3 and IrO_2 powders in a stoichiometric ratio of 1.1:1. The mixture was homogenized, pressed, and calcined in air for 24 h at 750 °C. Afterwards, it was again ground, pressed, and sintered for 72 h in 900 °C. Unfortunately, the target was rather soft. To improve it, attempts were made to employ high pressure sintering (HPS). However, the reducing conditions, due to the graphite heater used in HPS, had a detrimental effect on the target composition.

The deposition procedure involved a nucleation layer grown with 300 laser pulses at 1 Hz, followed by other 30 000 pulses at 15 Hz. After deposition, the samples were annealed *in situ* at an oxygen partial pressure $p_{O2} = 800$ mbar. Film thickness was estimated at ≈400 nm by spectroscopic ellipsometry. The growth process was optimized with respect to high film crystallinity, i.e., high x-ray diffraction (XRD) peak intensity. We have grown films at growth temperatures and oxygen partial pressures within the ranges from 550 °C to 700 °C, and from 0.1 mbar to 3.0×10^{-4} mbar, respectively. We note that for larger deposition temperatures Li_2IrO_3 films decomposed as indicated by additional x-ray reflexes belonging to other phases, most likely Ir_xO_y species. For these films, an energy dispersive x-ray (EDX) analysis gave a reduced Ir:O ratio of 1:2.13. Optimized films were grown at 600 °C and 3.0×10^{-4} mbar.

Investigations of the epitaxial relationship were performed with both a Panalytical X'Pert PRO Materials Research Diffractometer with parabolic mirror and PIXcel^{3D} detector and a Philips X'Pert x-ray diffractometer equipped with a Bragg-Brentano powder goniometer using divergent/focusing slit optics and Cu K_α radiation. Surface morphology was investigated via a Park System XE-150 atomic force microscope (AFM) in dynamic non-contact mode and a CamScan CS44 scanning electron microscope (SEM). Temperature dependent dc electrical resistivity was measured in van-der-Pauw geometry with dc magnetron-sputtered ohmic gold contacts. The DF was determined via standard variable angle spectroscopic ellipsometry in the spectral range from 0.03 to 3.34 eV: (IRSE). Infrared optical transmission in the spectral range from 0.14 to 1.30 eV was measured using a BRUKER IFS 66v/S FTIR in transmission mode (T-FTIR).

III. RESULTS AND DISCUSSION

A. Crystal structure

A typical XRD 2Θ-ω pattern of a Li_2IrO_3 film is shown in Fig. 1(a). For confirmation of the preferential film orientations, the XRD pattern of the polycrystalline PLD target is underlayed. The patterns are indexed on the basis of a monoclinic $C2/c$ unit cell.[5,18] The pattern shows pronounced symmetric peaks related to the (001) and (10–1) planes of the Li_2IrO_3 phase, see blue labels in Fig. 1(a). The intensity ratio $I_{(002)}/I_{(20-2)}$ is about 2.3:1 and thus much smaller than in the polycrystalline target (≈14:1). This strongly suggests preferential (001) and (10–1) out-of-plane crystalline orientations. However, peak assignment can be ambiguous, since in the monoclinic unit cell of Li_2IrO_3 many reflexes such as (20–2) and (004) are narrowly spaced. We fit the peak at

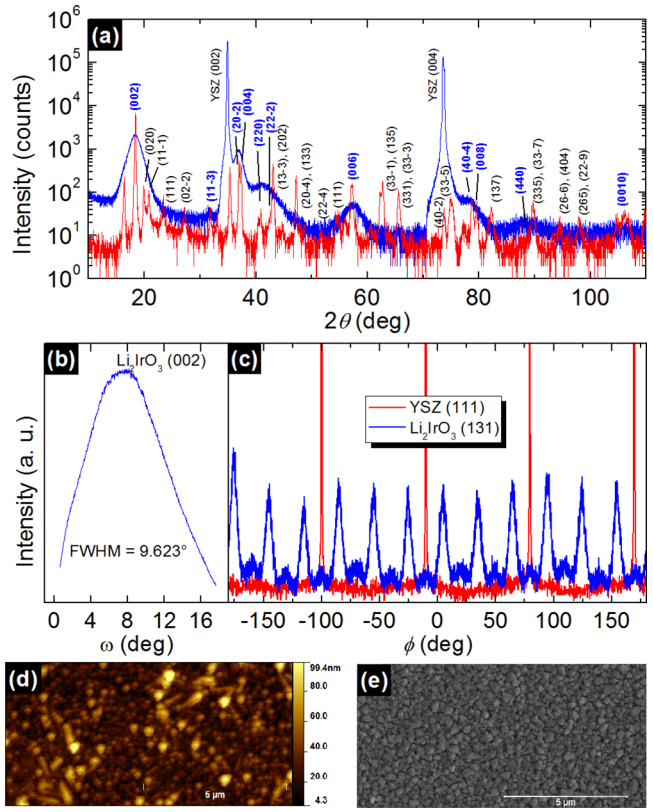

FIG. 1. (a) Typical XRD 2Θ-ω scan of a PLD-grown Li_2IrO_3 thin film on ZrO_2:Y (001) (YSZ) in blue, underlayed with the pattern of the polycrystalline PLD target in red. Significant film reflexes are labeled in blue. (b) Rocking curve about the (002) plane of Li_2IrO_3. (c) XRD ϕ-scans of asymmetric Li_2IrO_3 (131) and YSZ (111) reflections of the Li_2IrO_3(001) phase. (d) and (e) The surface morphology of the film is illustrated by non-contact AFM topographic and scanning electron microscopy images.

$2\Theta = 36.88°$ with two Gaussians to obtain d_{20-2} and d_{004}. From the d_{001} values of the (002), (004), and (006) reflexes, the c lattice parameter is determined as 9.71(1) Å. We also performed 2Θ–ω scans of the asymmetric (202) and (131) reflexes of the (001)-oriented phase and calculated lattice parameters $a = 5.20(3)$ Å and $b = 8.99(14)$ Å. For the calculations, we assumed $\beta = 99.992°$.[18] The lattice parameters are in good agreement with reported values,[5,18] a, b, and c deviating by +0.6%, +0.7%, and −0.8%, respectively. This indicates some amount of internal rather than epitaxial strain considering the significant lattice mismatch to YSZ (001).

A rocking curve of the (002) reflex at $2\Theta = 18.29°$ gives a full width at half maximum of about 10° (cf. Fig. 1(b)).

Investigation of the in-plane epitaxial relationship is done by x-ray diffraction ϕ-scans of the asymmetric Li_2IrO_3 (131) reflex of the (001)-oriented phase and of YSZ (111), shown in Fig. 1(c). For YSZ (001), we observe the C_4-symmetry of its (111) planes as expected. The ϕ-scan of the Li_2IrO_3 (131) reflection shows 12 + 12 reflections spaced by 15° alternating between "high" and "low" intensity peaks. Their intensity ratio is approximately 7:1. In Li_2IrO_3, the asymmetric (131) plane of both the (001)- and (10–1)-oriented phases share very similar angles. We therefore believe that the ϕ-scan shows the rotational domains of both phases. Thus, it indicates that the C_1-symmetric (monoclinic) (001)- and (10–1) oriented Li_2IrO_3 epilayers align in-plane within

12 rotational domains each. From the mismatch of rotational symmetry of substrate and epilayer,[30] we expect a minimum of four rotational domains. The origin of the increased number of rotational domains is at present unknown. One explanation might however be possible: Initially, Li_2IrO_3 was reported as pseudo-hexagonal.[20] If it occurred, the existence of epitaxially induced C_6-symmetry would lead, according to Ref. 30, to two rotational domains and thus 12 reflections in total per phase. Based on our x-ray data, it is not possible to determine the actual crystal structure of the epilayer, as the (001) planes of both monoclinic and pseudohexagonal symmetries share similar 2Θ angles. Epitaxially induced change of lattice symmetry was, e.g., observed for the growth of U_3O_8 on c-plane Al_2O_3.[31]

B. Chemical analysis and surface morphology

A qualitative elemental investigation of a film using secondary neutral mass spectrometry (SNMS) showed only Li, Ir, and O. An accumulation of volatile Li at the film-substrate interface was observed by SNMS depth profiling. However, it is currently not clear if the Ar^+-sputtering in SNMS contributes to this Li accumulation at the interface. Energy dispersive x-ray analysis gave an oxygen deficient Ir:O ratio of 1:2.84 under the optimized PLD conditions, as discussed above. This ratio points to possible oxygen vacancies, that might, in turn, explain the internal strain observed in XRD.

Figures 1(d) and 1(e) show topographic images of the Li_2IrO_3 film surface obtained with non-contact AFM and SEM, respectively. The images reveal a granular surface with an RMS roughness of 15.7 nm and a peak-to-valley height of 139.0 nm. The surface morphology can be explained by the presence of two preferential orientations and furthermore by the mechanically soft target promoting grain agglomeration. We have in fact tried growing films on lattice-matched $YAlO_3$ (011) single crystals but observed no improvement in either crystalline structure or surface morphology.

C. Electrical resistivity

As illustrated in Fig. 2, Li_2IrO_3 exhibits semiconducting resistivity behavior between 300 and 25 K. Resistivity does not follow a simple activated law $\rho \propto \exp(-\Delta/T)$, see inset of Fig. 2(a), which can also be associated with nearest-neighbor hopping. Instead, resistivity follows a $\rho \propto \exp[(\Delta/T^{1/4})]$ dependence down to at least 60 K. We associate this behavior to three-dimensional Mott VRH, as similarly observed in Na_2IrO_3 thin films.[19] Variable range hopping conduction results from localized states within a narrow energy band near the Fermi energy. At lower temperatures, resistivity diverges from this VRH dependence. As indicated by a straight line fit in inset of Fig. 2(b), we fit the resistivity data from 300 to 57 K with the three-dimensional Mott VRH model[32]

$$\rho = \rho_0 \exp[(T_0/T)^{1/4}], \tag{1}$$

where ρ_0 is a temperature-dependent resistivity coefficient and T_0 is the localization temperature. From the analysis of

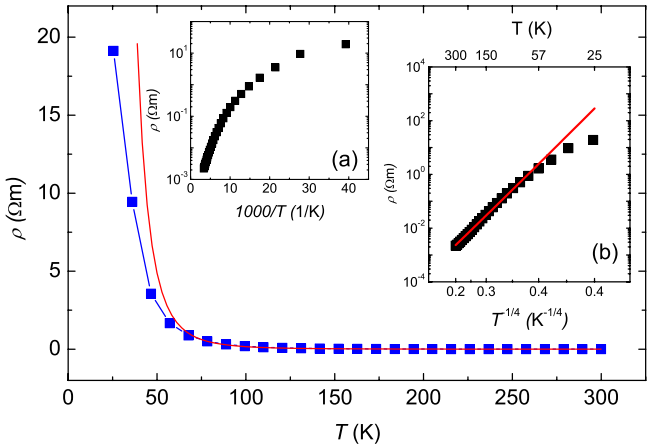

FIG. 2. Temperature-dependent resistivity ρ versus temperature T. The red line is a fit according to Eq. (1). Inset (a) shows $\log\rho$ versus $1000/T$. In inset (b) the data are plotted in $\log\rho$ versus $T^{-1/4}$. Red straight line fit with slope T_0 illustrates dominant three-dimensional Mott variable range hopping conductivity mechanism.

variable range hopping within percolation theory, the resistivity coefficient is given by[33,34]

$$\rho_0 = \rho_0'(T/T_0)^s, \tag{2}$$

where $s \approx 1/4$. Fitting Eq. (1) to the resistivity data, we extract $\rho_0' = 20(4) \times 10^{-8}\,\Omega\,\mathrm{m}$ and a localization temperature of $T_0 = 1.26(6) \times 10^7\,\mathrm{K}$. An estimate for the localization length a can be obtained from T_0 according to[33]

$$T_0 = 212/k_B a^3 N(E_F), \tag{3}$$

provided that $N(E_F)$, the density of states at the Fermi level, is known. Based on available heat capacity data of Li_2IrO_3 and Na_2IrO_3 single crystals,[5] we assume $N(E_F) \sim 10^{28}\,\mathrm{eV}^{-1}\,\mathrm{m}^{-3}$ (for details, see Ref. 19). The calculated localization length a is about 1.25(2) Å. Its magnitude is comparable with the Ir-Ir and Ir-O bond distances (approx. 3 and 2 Å, respectively) in the structurally very similar sister compound Na_2IrO_3,[15,17] supporting the applicability of Mott VRH. A criterion for the validity of Mott VRH is that the average hopping distance R_M be larger than the localization length a,[35] i.e.,

$$\frac{R_M}{a} = \frac{3}{8}\left(\frac{T_0}{T}\right)^{1/4} > 1. \tag{4}$$

The ratio R_M/a is equal to 5.37(7) at 300 K satisfying above criterion. We also verify that the maximal hopping distance R_{max} is much larger than the film thickness to exclude Mott VRH with hopping exponent 1/3. This kind of hopping is expected for thin films with thickness t in the order of the maximal hopping distance[36]

$$R_{max} = \frac{a}{2}\left(\frac{T_0}{T}\right)^{1/4}. \tag{5}$$

Using the estimated localization length a, we obtain a maximal hopping distance of $R_{max} = 1.36(4)$ nm at 57 K which is much smaller than the film thickness $t \approx 400$ nm.

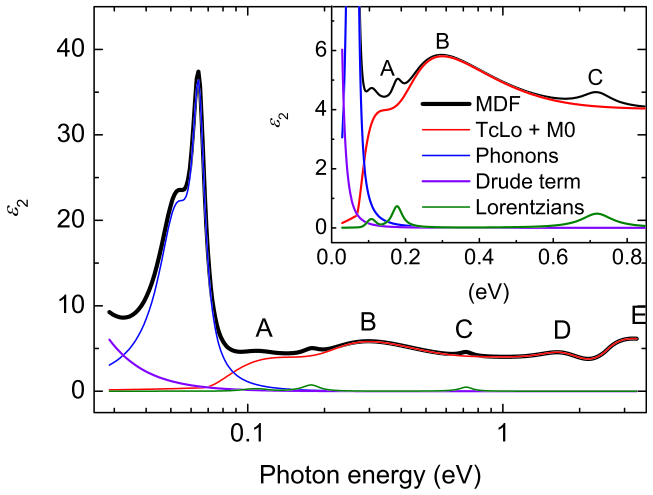

FIG. 3. Model dielectric function (MDF) and its individual components as obtained by spectroscopic ellipsometry of a Li_2IrO_3 thin film on YSZ(001). Labels *A*–*E* denote electronic excitations, see text and Table I. The inset shows a zoom-in on the electronic excitations below 0.8 eV.

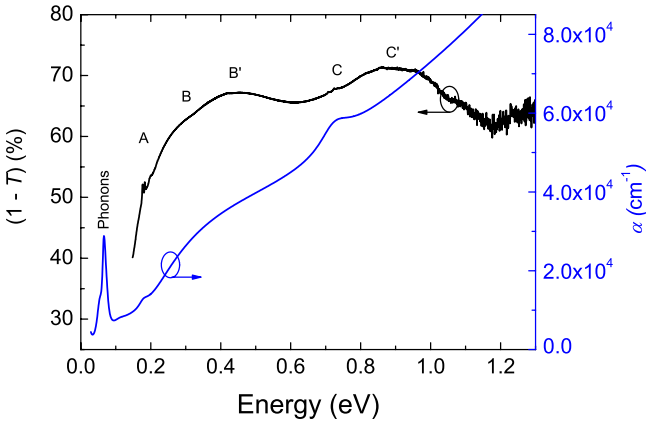

FIG. 4. Optical transmission (1-*T*) measured by T-FTIR (black) and optical absorption coefficient α (blue) of a Li_2IrO_3 thin film calculated from the MDF at ambient conditions. Labels *A*–*C*′ denote relevant excitations related to, e.g., *d*-*d* transitions.

D. Spectroscopic ellipsometry

Spectra of the DF were determined from the ellipsometry data by using a model containing a layer for the substrate, a layer for the Li_2IrO_3 film and a surface roughness layer. Each layer is described by its thickness and optical constants. Between the substrate and the Li_2IrO_3 thin film, a thin interface layer of about 1 nm was introduced by mixing 50:50 the substrate and film DF in a ratio of 1:1 by means of a Bruggeman effective-medium approximation (EMA).[37] Also, the surface roughness layer and the columnar structure was accounted for by a 100 nm EMA-layer by mixing the film DF with void. The void fraction was gradually increased from ≈20% to ≈80% from bottom to top (please cf. note Ref. 38). For modelling the thin film's DF, we used a parametric model DF (MDF) approach consisting of (cf. Fig. 3): A Drude free charge carrier absorption and two Lorentzians describing the phonon contribution at lowest energies; a near band gap Tauc-Lorentz (TcLo) absorption function[39] and a series of M0-critical point functions with parabolic onset[40,41] describing direct band-band transitions; Gaussian oscillators were used to model electronic band-band transitions spread within the Brillouin zone at higher energies. Additional discrete transitions where described by Lorentzians. Regression analysis was then applied to best match the dielectric function model to the experimental data. From the MDF, the absorption coefficient α was calculated (cf. Fig. 4).

The final MDF together with its individual components is displayed in Fig. 3. In the following, we argue that these individual components represent electronic excitations that can be ascribed to transitions from and within the t_{2g} manifold in line with the picture of j_{eff} physics, as explained earlier in the text. We also show that their transitions energies agree well with other experiments, such as angle-resolved photoemission spectroscopy (ARPES), RIXS, and optical spectroscopy, performed on Li_2IrO_3, Na_2IrO_3, and other iridates. The observed excitations are summarized in Table I.

In the high-energy spectral range above 1.2 eV, we find two contributions to the MDF at 1.63 and 3.25 eV that are attributed to *d*-*d* band transitions from occupied t_{2g} to empty e_g bands (*D*, *E*). Very similar transitions have been observed in Na_2IrO_3 and Li_2IrO_3 single crystals[21,42] and Na_2IrO_3 thin films.[19] Below 1.2 eV, we find several transitions. The transitions at 55 and 65 meV are attributed to phonons; at 0.11 and 0.18 eV we find discrete transitions (*A*). For example, in Sr_2IrO_4 a magnon was found at 0.2 eV within the Mott gap.[43] Further band-band excitations, possibly related to the particle-hole continuum boundary,[21] are found at 0.15 and more pronounced at 0.30 eV (*B*). They imply a very narrow Mott gap of less than 0.3 eV. Narrow Mott gaps from 300 meV to 340 meV were also previously found in Na_2IrO_3 and Li_2IrO_3.[19,21,42] Another discrete transition can be recognized at 0.72 eV (*C*). It is assigned to t_{2g} intraband transitions from $j_{\text{eff}} = 3/2$ to $j_{\text{eff}} = 1/2$ states. Excitations similar to *C* were found in other iridates, as well.[21,26,43]

E. Infrared transmission spectroscopy

A transmission spectrum of the film *T* was calculated from that of the entire sample T_{sample} and the substrate $T_{\text{substrate}}$, measured each by means of T-FTIR, via $T_{\text{sample}} \times 100/T_{\text{substrate}}$.[44] The (1–*T*) spectrum (Fig. 4) also reveals a narrow optical gap

TABLE I. Overview of electronic excitations energies in Li_2IrO_3 thin films determined by IRSE and T-FTIR. The uncertainty is in the order of the last digit.

Peak	*A*	*B*	*B*′	*C*	*C*′	*D*	*E*
Energy (eV)	0.11, 0.18	0.3	0.43	0.72	0.89	1.63	3.25
Type of excitation	Magnon (discrete)	$j_{\text{eff}} = 3/2 \rightarrow j_{\text{eff}} = 1/2$ (discrete)	$j_{\text{eff}} = 3/2 \rightarrow j_{\text{eff}} = 1/2$ (band-band)	$j_{\text{eff}} = 3/2 \rightarrow j_{\text{eff}} = 1/2$ (discrete)	$j_{\text{eff}} = 3/2 \rightarrow j_{\text{eff}} = 1/2$ (discrete)	$t_{2g} \rightarrow e_g$ (band-band)	$t_{2g} \rightarrow e_g$ (band-band)

below 0.3 eV. Furthermore, two broad peaks with shoulders can be discerned indicating electronic excitations. To compare with the IRSE data, the absorption coefficient α, calculated from the MDF, is included in Fig. 4 (blue curve) and the peak positions from Table I are indicated. Transitions *A*–*C* are reproduced in the T-FTIR data but are, however, complemented by transitions B' and C' (see Table I).

IV. SUMMARY

In summary, we have grown Li_2IrO_3 thin films by means of PLD on YSZ (001) substrates. XRD confirms that the films exhibit preferential (001) and (10–1) out-of-plane crystalline orientations with well defined in-plane orientation. Resistivity is dominated by three-dimensional variable range hopping. Electronic excitations below 3.34 eV were investigated via spectroscopic ellipsometry and transmission FTIR spectroscopy. On the basis of the j_{eff} physics and by comparison with related iridates, these excitations were associated to *d*-*d* transitions, transitions across the Mott gap and in-gap states. The optical gap was found to be ≈300 meV, smaller than that of Na_2IrO_3 films.

ACKNOWLEDGMENTS

We thank the Deutsche Forschungsgemeinschaft (DFG) for financial support within the project LO790/5-1 "Oxide topological insulator thin films." We are grateful to Yvonne Joseph and Uwe Sczech of Institut für Elektronik- und Sensormaterialien, TU Freiberg for high pressure sintering of PLD targets.

[1]A. Kitaev, Ann. Phys. **321**, 2 (2006).
[2]G. Jackeli and G. Khaliullin, Phys. Rev. Lett. **102**, 017205 (2009).
[3]J. Chaloupka, G. Jackeli, and G. Khaliullin, Phys. Rev. Lett. **105**, 027204 (2010).
[4]J. Reuther, R. Thomale, and S. Trebst, Phys. Rev. B **84**, 100406 (2011).
[5]Y. Singh, S. Manni, J. Reuther, T. Berlijn, R. Thomale, W. Ku, S. Trebst, and P. Gegenwart, Phys. Rev. Lett. **108**, 127203 (2012).
[6]J. Reuther, R. Thomale, and S. Rachel, Phys. Rev. B **90**, 100405 (2014).
[7]A. Shitade, H. Katsura, J. Kuneš, X.-L. Qi, S.-C. Zhang, and N. Nagaosa, Phys. Rev. Lett. **102**, 256403 (2009).
[8]D. Pesin and L. Balents, Nat. Phys. **6**, 376 (2010).
[9]C. H. Kim, H. S. Kim, H. Jeong, H. Jin, and J. Yu, Phys. Rev. Lett. **108**, 106401 (2012).
[10]H.-S. Kim, C. H. Kim, H. Jeong, H. Jin, and J. Yu, Phys. Rev. B **87**, 165117 (2013).
[11]A. Kitaev, Ann. Phys. **303**, 2 (2003).
[12]G. P. Collins, Sci. Am. **294**, 56 (2006).
[13]C. Nayak, A. Stern, M. Freedman, and S. D. Sarma, Rev. Mod. Phys. **80**, 1083 (2008).
[14]Y. Singh and P. Gegenwart, Phys. Rev. B **82**, 064412 (2010).
[15]F. Ye, S. Chi, H. Cao, B. C. Chakoumakos, J. A. Fernandez-Baca, R. Custelcean, T. F. Qi, O. B. Korneta, and G. Cao, Phys. Rev. B **85**, 180403 (2012).
[16]X. Liu, T. Berlijn, W.-G. Yin, W. Ku, A. Tsvelik, Y.-J. Kim, H. Gretarsson, Y. Singh, P. Gegenwart, and J. P. Hill, Phys. Rev. B **83**, 220403 (2011).
[17]S. K. Choi, R. Coldea, A. N. Kolmogorov, T. Lancaster, I. I. Mazin, S. J. Blundell, P. G. Radaelli, Y. Singh, P. Gegenwart, K. R. Choi, S.-W. Cheong, P. J. Baker, C. Stock, and J. Taylor, Phys. Rev. Lett. **108**, 127204 (2012).
[18]H. Kobayashi, M. Tabuchi, M. Shikano, H. Kageyama, and R. Kanno, J. Mater. Chem. **13**, 957 (2003).
[19]M. Jenderka, J. Barzola-Quiquia, Z. Zhang, H. Frenzel, M. Grundmann, and M. Lorenz, Phys. Rev. B **88**, 045111 (2013).
[20]H. Kobayashi, R. Kanno, M. Tabuchi, H. Kageyama, O. Nakamura, and M. Takano, J. Power Sources **68**, 686 (1997).
[21]H. Gretarsson, J. P. Clancy, X. Liu, J. P. Hill, E. Bozin, Y. Singh, S. Manni, P. Gegenwart, J. Kim, A. H. Said, D. Casa, T. Gog, M. H. Upton, H. S. Kim, J. Yu, V. M. Katukuri, L. Hozoi, J. van den Brink, and Y. J. Kim, Phys. Rev. Lett. **110**, 076402 (2013).
[22]I. I. Mazin, H. O. Jeschke, K. Foyevtsova, R. Valentí, and D. I. Khomskii, Phys. Rev. Lett. **109**, 197201 (2012).
[23]I. I. Mazin, S. Manni, K. Foyevtsova, H. O. Jeschke, P. Gegenwart, and R. Valentí, Phys. Rev. B **88**, 035115 (2013).
[24]S. Bhattacharjee, S.-S. Lee, and Y. B. Kim, New J. Phys. **14**, 073015 (2012).
[25]B. J. Kim, H. Jin, S. J. Moon, J. Y. Kim, B. G. Park, C. S. Leem, J. Yu, T. W. Noh, C. Kim, S. J. Oh, J. H. Park, V. Durairaj, G. Cao, and E. Rotenberg, Phys. Rev. Lett. **101**, 076402 (2008).
[26]S. J. Moon, H. Jin, K. W. Kim, W. S. Choi, Y. S. Lee, J. Yu, G. Cao, A. Sumi, H. Funakubo, C. Bernhard, and T. W. Noh, Phys. Rev. Lett. **101**, 226402 (2008).
[27]H. Kuriyama, J. Matsuno, S. Niitaka, M. Uchida, D. Hashizume, A. Nakao, K. Sugimoto, H. Ohsumi, M. Takata, and H. Takagi, Appl. Phys. Lett. **96**, 182103 (2010).
[28]Y. S. Lee, S. J. Moon, S. C. Riggs, M. C. Shapiro, I. R. Fisher, B. W. Fulfer, J. Y. Chan, A. F. Kemper, and D. N. Basov, Phys. Rev. B **87**, 195143 (2013).
[29]S. J. Moon, M. W. Kim, K. W. Kim, Y. S. Lee, J. Y. Kim, J. H. Park, B. J. Kim, S. J. Oh, S. Nakatsuji, Y. Maeno, I. Nagai, S. I. Ikeda, G. Cao, and T. W. Noh, Phys. Rev. B **74**, 113104 (2006).
[30]M. Grundmann, T. Böntgen, and M. Lorenz, Phys. Rev. Lett. **105**, 146102 (2010).
[31]A. K. Burrell, T. M. McCleskey, P. Shukla, H. Wang, T. Durakiewicz, D. P. Moore, C. G. Olson, J. J. Joyce, and Q. Jia, Adv. Mater. **19**, 3559 (2007).
[32]N. F. Mott, Philos. Mag. **19**, 835 (1969).
[33]B. Shklovskii and A. Efros, *Moscow Izdatel Nauka* (Springer, Berlin, Heidelberg, New York, Tokyo, 1984).
[34]N. Arginskaya and V. Kozub, Zh. Eksp. Teor. Fiz. **106**(3), 848 (1994).
[35]N. Mott, J. Non-Cryst. Solids **1**, 1 (1968).
[36]V. Shante, Phys. Lett. A **43**, 249 (1973).
[37]G. E. Jellison, L. A. Boatner, D. H. Lowndes, R. A. McKee, and M. Godbole, Appl. Opt. **33**, 6053 (1994).
[38]Please note that such a high surface roughness cannot be exactly described by this approach and the DF of the surface layer with their chosen gradient strongly correlates with the DF of the thin film. Therefore, for absolute values of the thin film DF a uncertainty of $\Delta\varepsilon_2 \approx +20\%/-5\%$ in the worst case has to be taken into account. But nevertheless, their general lineshape and the energy values of the electronic excitations and phonon modes are influenced far less and are therefore reliable. For the same reason we do not report ε_1 because here the error amounts up to 50%.
[39]G. E. Jellison and F. A. Modine, Appl. Phys. Lett. **69**, 371 (1996).
[40]S. Adachi, Phys. Rev. B **35**, 7454 (1987).
[41]H. Yoshikawa and S. Adachi, Jpn. J. Appl. Phys., Part 1 **36**, 6237 (1997).
[42]R. Comin, G. Levy, B. Ludbrook, Z. H. Zhu, C. N. Veenstra, J. A. Rosen, Y. Singh, P. Gegenwart, D. Stricker, J. N. Hancock, D. van der Marel, I. S. Elfimov, and A. Damascelli, Phys. Rev. Lett. **109**, 266406 (2012).
[43]J. Kim, D. Casa, M. H. Upton, T. Gog, Y.-J. Kim, J. F. Mitchell, M. van Veenendaal, M. Daghofer, J. van den Brink, G. Khaliullin, and B. J. Kim, Phys. Rev. Lett. **108**, 177003 (2012).
[44]The reflectivity of the thin film and the substrate is almost constant in that range and small, thus neglecting both introduces an error of less than 5% in *T*.